3

Synthesis of Titanate and Titanium Dioxide Nanotube Thin Films and Their Applications to Biomaterials

Mitsunori Yada and Yuko Inoue
Saga University
Japan

1. Introduction

Recently, titanium compounds with one-dimensional nanostructures, such as nanotubes and nanofibers, have recently attracted much attention. Among these 1-D compounds, nanotubes composed of titanium dioxide and titanate are now being studied actively. Titanium dioxide nanotubes can be synthesized using porous anodic alumina membranes (Imai et al., 1999; Yamanaka et al., 2004), organic molecules (Jung et al., 2002), or polycarbonate membranes (Shin et al., 2004) as templates, or methods involving anodization of titanium metals (Macak et al., 2005). Since the interesting reports by Kasuga et al. (Kasuga et al., 1998; Kasuga et al., 1999) and Chen et al. (Chen et al., 2002), titanate and titanium dioxide nanotubes synthesized using the hydrothermal method have found a wide range of potential uses in photocatalysis (Tokudome et al., 2004; Jiang et al., 2008), dye sensitizing solar batteries (Uchida et al., 2002), hydrogen storage (Bavykin et al., 2005), electrochromism (Tokudome et al., 2005), bonelike apatite formation (Kubota et al., 2004), proton conductors (Thorne et al., 2005), electron field emission characteristic (Miyauchi et al., 2006), photoinduced hydrophilicity (Tokudome et al., 2004), etc.

In order to maximize the characteristics of the nanotube and to use them efficiently, preventing their excessive aggregation and arrangement at larger than micrometer or centimeter size are considered important. Especially, it is important to fabricate thin films composed of nanotubes. Kasuga et al. (Kasuga et al., 2003) reported the fabrication of titanate nanotube thin films by coating a titanate nanotube dispersion liquid to a substrate, and then calcinating the substrate. Tokudome et al. (Tokudome et al., 2004) and Ma et al. (Ma et al., 2004) also reported the fabrication of titanate nanotube thin films using a layer-by-layer method. However, neither study had transformed titanate nanotube thin films into titanium dioxide thin films. Kim et al. (Kim et al., 2007) used electrophoretic deposition (EPD) to fabricate 2-μm-thick titanate nanotube thin films, and they transformed the titanate nanotube thin films into titanium dioxide nanotube thin films by calcination. However, these methods involve complicated processes, including (1) synthesis of nanotubes, (2) preparation of a liquid in which the synthesized nanotubes are dispersed, (3) coating of the nanotubes onto a substrate using the prepared liquid, and (4) fixation of the coated nanotubes onto the substrate surface by calcination. Since it is generally difficult to prepare

a liquid in which nanotubes are uniformly dispersed and that partial aggregation is inevitable, the homogeneity of thin films thus formed is questionable. Moreover, permanent fixation of the thin films onto the substrates is also doubtful. On the other hand, titanate and titanium dioxide nanotube thin films can also be formed on titanium metal by immersing titanium metal as a raw material into NaOH aqueous solution and then performing hydrothermal treatment (Miyauchi et al., 2006; Tian et al., 2003; Chi et al., 2007; Yada et al., 2007; Guo et al., 2007). The fabrication of titanate nanotube thin films using titanium metal plates was first reported by Tian et al. (Tian et al., 2003). The thin (~10 μm) films were detached from the titanium metal plates by hydrothermal reaction for 20 h. In contrast, thin films obtained by a short (6 h) hydrothermal reaction strongly adhered to the titanium metal plate. Miyauchi et al. (Miyauchi et al. 2006) obtained a titanium dioxide nanotube thin film by hydrothermal treatment on titanium metal, followed by acid treatment and calcination. Although this thin film was fixed onto the substrate, its thickness was only a few hundred nanometers. Therefore, it is clear that titanate and titanium dioxide nanotube thin films tend to detach from the substrates when they become too thick. Chi et al. also reported the fabrication of a sodium titanate nanotube thin film (Chi et al., 2007). However, the thickness of the film was not mentioned in their report, and the sodium titanate nanotubes were not transformed into titanium dioxide nanotubes.

In this chapter, first, we will report the synthesis and organization of sodium titanate nanotube (hereafter referred to as Na-TNT) of size larger than a micrometer, using various titanium metals with controlled shapes of a micrometer size including plate, wire with a diameter of a micrometer, mesh woven from the titanium wire, microspheres, and microtube (Yada et al., 2007). The titanium metal acts as a template for the organization as well as a titanium source. Therefore, the originality of our study is to use titanium metal as a morphology-directing material. In addition, we will report a novel procedure for fixation of Na-TNT thin film on titanium metal (Yada et al., 2007). As a result, the thickness of the sodium titanate nanotube thin film can be adjusted by changing the duration of the hydrothermal reaction and the obtained films are thicker than those reported in previous studies (Miyauchi et al., 2006; Tian et al., 2003). Furthermore, we will also introduce a novel "hydrothermal transcription method" for forming Na-TNT films on various substrates such as Co-Cr alloy and SUS316L (Yada et al., 2008). Transformation of Na-TNT thin films into thin films consisting of anatase nanotube, anatase nanowires, anatase nanoparticles, and rhomboid-shaped anatase nanoparticles are also introduced (Inoue et al. 2010). To obtain an anatase nanotube thin film, it is necessary to slightly modify previously reported methods for synthesizing titanium dioxide nanotube particles.

Next, in this chapter, obtained titanate and titanium dioxide nanotube thin films will be applied to antibacterial biomaterials (Inoue et al., 2010). The nanotube thin film has several advantages: it can be formed on titanium, titanium alloy, Co–Cr alloy, and SUS316L, which are useful for manufacturing surgical instruments and implants such as artificial joints; its thickness can be controlled up to 20 μm or more, in contrast to only 1 μm for the thickness of the previously reported sodium titanate thin film with a porous network structure; and medicines can be incorporated into the nanotube. It is well known that bacterial infection may occur during surgery because of several factors. For example, during hip-replacement arthroplasty, bacterial infections occur in 1% to 2% of operations and usually cause physical and economic burdens for patients, such as re-implantation. As a conventional method for

preventing infections, antibiotics are administered even in operation rooms with few pathogens. However, this does not prevent every infection. Therefore, imparting antibacterial properties to implants is currently under investigation. There have been reports of the use of apatite coating containing silver on implants by sputtering (Chen et al., 2006), silver-plated implants (Hardes et al., 2007), and gentamicin–hydroxyapatite coating for cementless joints (Alt et al., 2006), all of which have shown antibacterial properties. However, these methods have drawbacks such as the need for expensive instruments and the use of antibiotics that may cause the emergence of resistant bacteria. Therefore, further research is required. In this study, in order to develop more convenient and inexpensive antibacterial implants, silver ions are studied as an antibacterial component along with titanate nanotube formed on the surface of titanium. Silver is one of the most common antibacterial elements and is considered highly safe with high antibacterial activity. Sodium titanates are composed of a titanate framework with a negative electric charge and Na^+ ions with a positive electric charge. Since they have a cation exchange property, Na^+ ions can be exchanged with several cations (Kim et al., 1997; Chen et al., 2002; Sun et al., 2003; Bavykin et al., 20006). Therefore, it is considered that sodium titanate can be transformed into silver titanate by exchange of Na^+ in sodium titanate with Ag^+, and the in vivo elution of silver ions from the titanates would be promising for application to antibacterial implants. In addition, it is suggested that the titanate nanotube thin film would be able to possess a larger amount of silver and allow the amount of silver to be controlled more widely as compared with the titanate thin film previously reported (Kim et al., 1996). In this chapter, we will describe the synthesis and characterization of titanate nanotube thin films with silver and the behavior of silver ion elution of the thin films in vitro. We will also describe the antibacterial properties against methicillin-resistant Staphylococcus aureus (MRSA) with a biofilm-forming gene, which is a major concern in actual infections, to investigate the possibility of using synthesized thin films as antibacterial implants.

Finally, we will describe the apatite-forming abilities of titanium compound nanotube thin films by comparing the apatite deposition behaviors of a sodium titanate nanotube thin film (Yada et al., 2007), a titanium dioxide nanotube thin film (Inoue et al., 2010), and a silver nanoparticle/silver titanate nanotube nanocomposite thin film (Inoue et al., 2010), in simulated body fluid (SBF) (Yada et al., 2010). In evaluating the in vivo apatite-forming ability or the osteoconductive property of a material, researchers commonly perform experiments in SBF (Kokubo et al., 2006)). Kim et al. (Kim et al., 1996) first reported the formation of a sodium titanate thin film with a porous network structure on a titanium metal plate by alkali and heat treatment and demonstrated the osteoconductive property of the obtained sodium titanate thin film. Since then, researchers have actively performed many studies on the applications of sodium titanate thin films in implants (Kokubo et al., 1996; Kim et al., 1997; Kim et al., 1997; Nishiguchi et al., 1999; Jonášová et al., 2003; Kim et al., 2003; Muramatsu et al., 2003; Wang et al., 2007; Wang et al., 2008). Similar studies have also been performed on calcium titanate thin films (Hanawa et al., 1997; Hamada et al., 2002; Nakagawa et al., 2005; Kon et al., 2007; Ohtsu et al., 2008), titanium dioxide thin films (Ohtsuki et al., 1997; Wang et al., 2001; Wang et al., 2003; Byon et al., 2007), and a nanohydroxyapatite thin film (Xiong et al., 2010), and the excellent biocompatibilities of these films have been reported. Therefore, titanium compound thin films show tremendous promise for use as implant materials.

2. Synthesis and characterization of titanate and titanium dioxide nanotube thin films

2.1 Sodium titanate nanotube thin films formed on various shaped titanium metal templates

2.1.1 Sodium titanate nanotube thin film formed a titanium plate

First, the growth and fixation of Na-TNT on titanium plate were investigated. A titanium plate (20 mm × 20 mm × 2 mm) was immersed in 20 ml of 10 mol/l aqueous NaOH solution in a Teflon container and reactions were carried out at 160°C. After hydrothermal treatment for 20 h, the surface of the plate changed to pale, indicating the formation of a thin film on the titanium plate. In order to wash out NaOH and the particles that adhered to the surface of the thin film, the plate was washed with water after the reaction. The thin film immediately exfoliated as shown in Fig. 1a, and then a surface with a metallic luster similar to that of titanium metal appeared on the surface of the plate. The greater part of the film was posited to consist of nanotubes with an outer diameter of approximately 8 nm (Fig. 1b). Through EDX analysis, the mol fraction of Na/Ti/O for the obtained film was determined to be 1:1.947:4.943. The film was thus assumed to be $Na_2Ti_4O_9{\cdot}H_2O$, though some titanate structures, such as $A_2Ti_2O_5{\cdot}H_2O$ (Yang et al., 2003), $A_2Ti_3O_7$ (Chen et al., 2002), $H_2Ti_4O_9{\cdot}H_2O$ (Nakahira et al., 2004), and lepidocrocite titanates (Ma et al., 2003), have been assigned as nanotube constituents (A=Na and /or H) as summarized by Tasi et al (Tasi et al., 2006). Moreover, by detailed SEM observation of the cross-section of this film, the film thickness was determined to be approximately 20.2 μm, as shown in Fig. 1c. The thickness of the Na-TNT phase was determined to be approximately 19.2 μm, and the thickness of the dense sodium titanate phase without Na-TNT was determined to be approximately 1.0 μm. Although fibrous morphologies were observed on the surface of the film, the back of the film was flat with no visible fibers. Therefore, the film exfoliation was considered to occur at the interface between the titanium metal phase and the sodium titanate phase without Na-TNT. Based on the above results, the formation of the Na-TNT thin film can be explained as follows: (1) titanium dissolves into titanium ions (Ti^{4+}) by oxidizers, H^+ and/or O_2; (2) dissolved Ti^{4+} ions immediately form titanium species (Wu et al., 2006) such as TiO_3^{2-}, $TiO_2(OH)_2^{2-}$, and $Ti_nO_{2n+m}^{2m-}$ and the concentration of titanium species in the reaction solution increases as the dissolution of titanium is accelerated; (2) titanium species are reprecipitated as sodium titanate with an increase in the concentration of titanium species in the reaction solution; (3) since the concentration of the titanium species in the reaction solution is expected to increase with time, the sodium titanate phase without Na-TNT is formed when the concentration of titanium species is low and the Na-TNT phase is formed after the concentration becomes sufficiently high. The Na-TNT-free sodium titanate phase formed at low concentrations of titanium species may be amorphous sodium titanate. Since the concentration of titanium species in the reaction solution is considered to affect the type of sodium titanate cluster and the formation rate of the sodium titanate phase, the concentration of titanium species, together with temperature and other concentrations, are also considered to be factors in determining the type of phase formed.

Moreover, in order to prevent detachment of the thin Na-TNT film, the as-synthesized plate was slowly dried at room temperature after the hydrothermal treatment without washing it with water. Although NaOH crystals were observed on the plate, the thin film still adhered

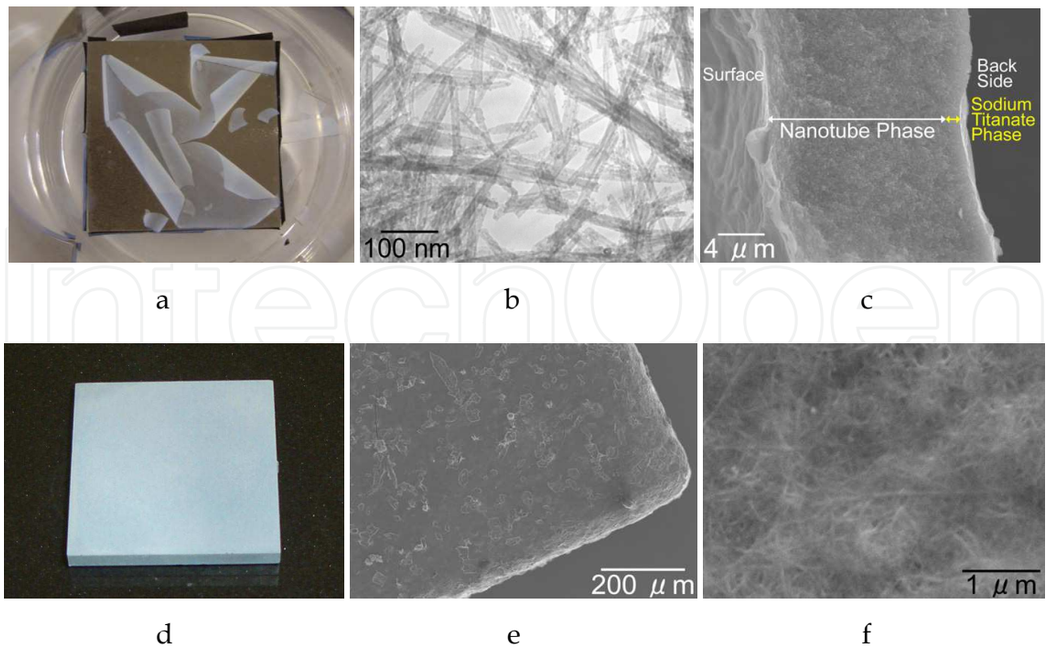

Fig. 1. Photograph (a, d), TEM (b), and SEM (c, e, f) images for the as-grown (a-c) and the 300 °C calcined (d-f) products obtained after the 20 h reaction.

to the plate. When the plate was washed with water after heat treatment at 300°C for 1 h in air, although the NaOH crystals dissolved, the thin Na-TNT film still adhered to the plate firmly and no detachment was observed as shown in Fig. 1d. Na-TNT formation was confirmed by the fibrous morphologies observed on the surface of the thin film in an enlarged SEM image (Figs. 1e, f) and nanotubes observed in a TEM image of the thin film. Moreover, in an XRD pattern of the thin film (Fig. 2), only diffraction peaks characteristic of Na-TNT (Chen et al., 2002) were observed along with peaks assigned to titanium metal. The reason for this stable coating is probably because polycondensation of hydroxyl groups in the interface area between the titanium plate and the Na-TNT-free sodium titanate phase occurred by the heat treatment at 300°C, and Na-TNT being firmly fixed on the plate. The slow drying process is also considered to be important for the fixation of Na-TNT onto the titanium plate, since the thin film detached from the titanium plate by drying at 60°C. The formation and fixation of the Na-TNT thin film were also observed in the reaction after 3 h. Nanotubular structures similar to those of the 20 h product were also observed. The thickness of approximately 5 μm for the film obtained after the 3 h reaction was smaller than that of 20.2 μm for the film obtained after the 20 h reaction. The thickness of the film is thus controllable by the reaction time. On the other hand, when an as-synthesized Na-TNT thin film obtained by hydrothermal reaction in 10 mol/L NaOH solution at 160 °C for 1 h was washed with large amounts of water, the Na-TNT thin film do not detach from the substrates and remains as thin as approximately 1 μm. Therefore, it is clear that sodium titanate nanotube thin films tend to detach from the substrates when they become too thick, but remain firmly fixed on substrates when the obtained samples are dried (without washing with water) and subsequently calcined at 300 °C.

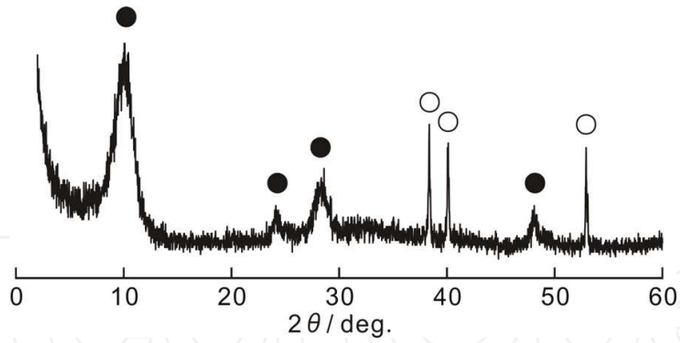

Fig. 2. XRD pattern for the plate obtained after the 20 h reaction. Peak assignment: ○ titanium metal, ● sodium titanate nanotube.

2.1.2 Sodium titanate nanotube thin films formed on titanium wire, titanium mesh, titanium sphere, and titanium microtube

Titanium wire (lengths: 5 cm, 24 cm, and diameters: 53.4 μm, 104.4 μm, 203.7 μm), titanium mesh (woven from the titanium wire with a diameter of 104.4 μm, 20 mm × 20 mm), titanium tube (inner diameter: 800 μm, outer diameter: 1 mm, length: 1 cm), and titanium spheres (diameter: 850–1180 μm, weight: 0.21-0.24 g) were used as metal titanium sources instead of a titanium plate.

After the hydrothermal treatments for 3 h and 20 h, the surfaces of titanium mesh and titanium sphere were completely covered with Na-TNT thin film. Both outer and inner surfaces of the microtube were also covered with uniform nanotubes with an average diameter of 8 nm. Typical digital camera and SEM images are shown in Figs. 3a-c.

On the other hand, the formation of Na-TNT thin film on a titanium wire requires special procedures which are different from those for plate, mesh, sphere, and microtube. First, the synthesis and fixation of Na-TNT were investigated using titanium metal wires of diameters 53.4 and 104.4 μm and length 5 cm as titanium sources. As a result, after the hydrothermal treatment for 3 h, sodium titanate with an irregular morphology was formed on the surface of the titanium wires, and only small amount of nanotubes was observed in the product synthesized using the titanium wire of diameter 104.4 μm. The diameters decreased from 53.4 and 104.4 μm for the original wires to 36.3 and 93.8 μm for the wires after a reaction time of 3 h, respectively. Moreover, after the hydrothermal treatment for 20 h, both wires completely dissolved. In addition, in the experiment using a wire of diameter 53.4 μm and length 24 cm, no nanotubes were observed on the surface of the obtained wire at a reaction time of 3 h and the wire completely dissolved at a reaction time of 20 h. On the other hand, in the experiment using a wire of diameter 104.4 μm and length 24 cm, the amount of Na-TNT formed increased at 3 h reaction time, and the surface of the wire was completely covered with Na-TNT thin film at the 20 h reaction. The reason for the complete dissolution of the original wires is because the dissolution rates of titanium species from the wires were faster than the redeposition rate of sodium titanate on the surface of the wires. On the other hand, the reason for the complete coverage of Na-TNT on the wire without dissolution is that the redeposition rate of sodium titanate nanotubes on the wire's surface became faster than the dissolution rate of titanium species from the wire with an increase in its diameter and length. These differences depending on the diameters of the original wires are

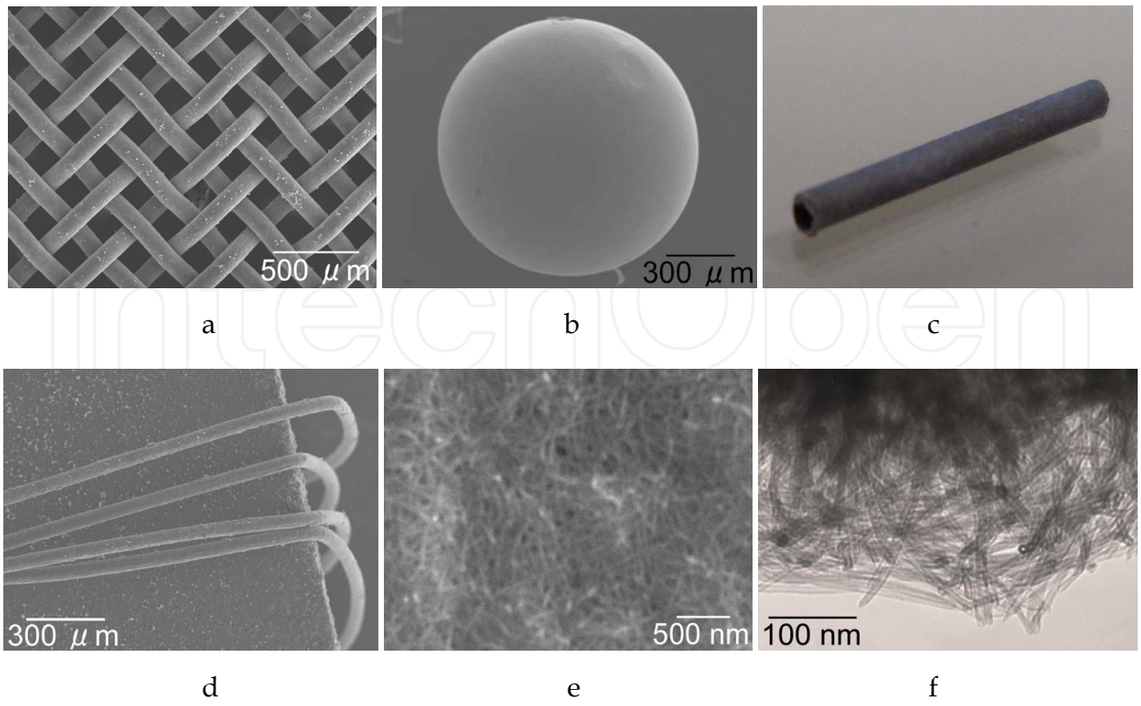

Fig. 3. SEM (a, b, d, e), Photograph (c), and TEM (f) images for the mesh (a), micro-sphere (b), microtube (c), and wire (d-f) obtained after the 3 h reaction.

explained as follows. Surface area and surface texture strongly affect the concentration of titanium species in the reaction solution. The amount of titanium species in the reaction solution increases with an increase in the diameter of the wire, since the surface area of the wire increases with an increase in the diameter. Additionally, the difference in the surface texture of the wires also affects the concentration of titanium species near their surfaces. Detailed SEM observations of the original titanium wires confirmed that the surfaces of the wire of diameter 104.4 μm were porous, but the surface of the wire of diameter 53.4 μm was relatively smooth. The concentration of titanium species would be higher near the wire and lower as the distance from the wire increases. In particular, the concentration of titanium species near the porous surface would be higher than that near the smooth surface. Therefore, in the experiments using the 104.4 μm diameter wire, the amount of titanium species formed per unit of time and the concentration of the titanium species would be large due to their larger diameters and porous surfaces, and consequently the concentration of titanium species would be sufficiently high for the formation of Na-TNT as the dissolution of titanium proceeded. On the other hand, since the surface area of the 53.4 μm diameter wire was predicted to be smaller than the 104.4 μm diameter wire due to its diameter and smooth surface, the concentration of titanium species formed per unit of time would also be small. Therefore, the concentration of titanium species would be too low for the formation of Na-TNT. Consequently, sodium titanate with irregular morphology was formed without Na-TNT at a reaction time of 3 h and the original wire completely dissolved at a reaction time of 20 h. Taking into consideration the above discussion, a similar hydrothermal and fixing treatment was performed using a wire of diameter 53.4 μm and length 24 cm wound onto the above mentioned titanium plate, which could act as a source of titanium species.

Wired morphologies remained for 3 h (Fig. 3d) and 20 h reactions, respectively, and the surfaces of both wires were completely covered with uniform Na-TNT thin films (Figs. 3e, f). It is considered that since the amount of titanium species reprecipitated on the wire, supplied by the dissolution from the titanium plate, was larger than the amount of titanium species dissolved from the wire, the surface of the wire was covered with Na-TNT. These results also indicate that dense concentration of titanium species near the titanium surface is required for the formation of Na-TNT on the titanium wire. Based on the above results, Na-TNT applications can be largely extended by the hydrothermal treatment of a cloth woven with titanium wires and by weaving a cloth with Na-TNT/Ti wires.

2.2 Sodium titanate nanotube thin films formed on Co–Cr alloy and SUS316L plates

We devised a "hydrothermal transcription method" for forming Na-TNT films on various substrates, as shown in Fig. 4. In this method, Na-TNT would be produced by re-depositing or transcribing the titanium species such as TiO_3^{2-}, $TiO_2(OH)_2^{2-}$, and $Ti_nO_{2n+m}^{2m-}$ formed near the surface of the titanium plate by hydrothermal treatment in aqueous NaOH solution on other substrate as Na-TNT, and grown to form dense films on several substrates as well as on the titanium plate. As shown in Fig. 4, under the conditions where a titanium metal plate and a substrate were adjacently placed, the titanium metal plate and substrate were spaced uniformly (about 200 μm) and fixed using titanium wires or SUS316 wires. For the substrate, Co–Cr alloy disk, SUS316L plate, SUS430 plate, tantalum plate, and silicon plate were used. These were immersed in 10 mol/l NaOH aqueous solution and reacted hydrothermally for 20 h at 160 °C. After the reaction, the samples were removed from the container and dried. Then, by washing in water following heat treatment at 300 °C, excessive NaOH adhered on the substrate was removed.

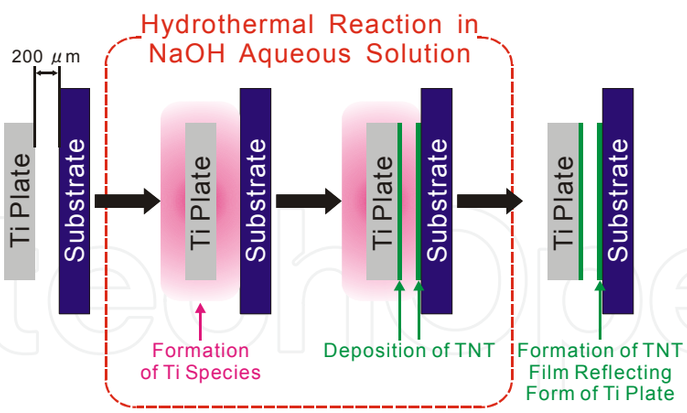

Fig. 4. Schematic representation of a reaction process by the hydrothermal transcription method.

Firstly, the Co–Cr alloy disk was used as a substrate. As shown in Fig. 5a, after the reaction, the formation of a white film whose base is the color of Co–Cr alloy along the square form of counter titanium plate on only the face countered to the titanium plate was observed. This white film strongly adhered to the Co–Cr alloy plate. By SEM images (Figs. 5b, c), the uniform and dense formation of fibrous substances was identified. Also by TEM observation of fibrous substances, nanotubes with an outer diameter of about 8 mm were identified (Fig.

5d). The thickness of this film is about 5 μm. This thickness was less than the 20 μm thickness of the Na-TNT film formed on the titanium plate when reacted singly (Yada et al., 2007). As the XRD pattern of the Co–Cr alloy surface countered to the titanium plate, a diffraction peak characteristic to titanate nanotube near 2θ = 10° as well as the peaks attributed to the Co–Cr alloy of the raw material were observed. From a EDX analysis, it was found that the film contains Na, Ti, O, Co, Cr, and Si, and the molar ratio for the film was Na:Ti:O:Co:Cr:Si=0.322:1:2.401:0.112:0.052:0.045. Sodium titanate nanotube film is thus thought to be formed on the Co–Cr alloy disk. The elements of Co, Cr, and Si would dissolve from the Co–Cr alloy disk and would be incorporated into the titanate framework and/or the interlayer spacing of the titanate. Furthermore, as observed above, the white Na-TNT film reflecting the square form of the titanium plate was observed on the Co–Cr alloy disk countered to the titanium plate (Fig. 5a). Thus, the titanium species capable of forming Na-TNT were present near the surface of titanium, and it can be considered that Na-TNT patterning reflecting the form of the titanium plate was made on the surface of the Co–Cr alloy disk countered to the titanium plate. The above results suggest that by using several forms of the titanium plate as the titanium source, several forms of Na-TNT patterning can be made on heterogeneous substrates.

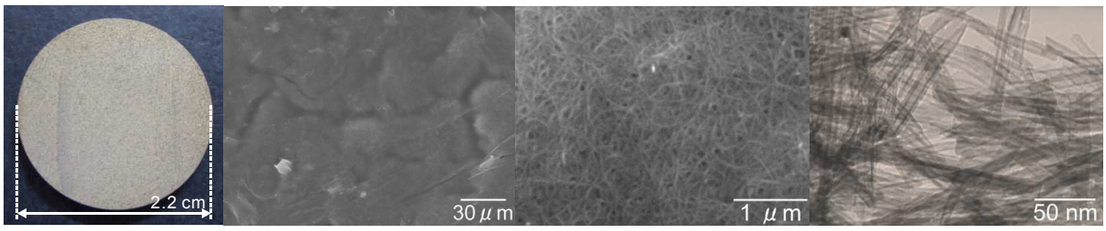

a b c d

Fig. 5. Digital camera (a), SEM (b, c), and TEM (d) images for the obtained thin film formed on the surface of Co-Cr alloy countered to titanium metal.

When the same experiment was conducted with SUS316L plate instead of the Co–Cr alloy disk, it was found that as in the case of Co–Cr alloy, diluted white Na-TNT thin film was formed on the surface of SUS316L plate countered to the titanium plate. On the other hand, when the same reaction was performed using the SUS430 plate instead of Co–Cr alloy disk, brown and black iron compounds were formed on the SUS430 plate, although white Na-TNT film was formed in part. SUS430 is an industrial grade stainless alloy, whereas SUS316L is a stainless alloy used in implants and has exceptionally high corrosion resistance, and the results reflecting this corrosion resistance were obtained. When the same reaction was performed with the tantalum plate instead of the Co–Cr alloy plate, copious amounts of white products were produced on the tantalum plate, and particles other than nanotubes were observed. In addition, when the same experiment was performed using a silicon plate instead of the Co–Cr alloy disk, the silicon plate was completely dissolved by the hydrothermal reaction. On considering the differences in the responsiveness of substrates, it is thought that the dissolution rate of the titanium plate and substrates and redeposition rate of chemical species that arose from the dissolved titanium plate and substrates should be considered. Particularly, in this experiment system, it is considered that the dissolution rate of substrates has a large effect on the results of the experiments. The dissolution rate of using metals as substrates, as in this study, can be explained by the

ionization tendency, i.e., oxidation–reduction potential. It is considered that titanium dissolves into titanium ions (Ti^{4+}) by oxidizers, H^+ and/or O_2, and these dissolved ions immediately form chemical species (Wu et al., 2006) such as TiO_3^{2-}, $TiO_2(OH)_2^{2-}$, and $Ti_nO_{2n+m}^{2m-}$ which are re-deposited as Na-TNT. When a substrate whose ionization tendency is smaller than titanium, especially materials such as SUS316L and Co–Cr alloy, is hydrothermally reacted with titanium simultaneously, the dissolution rate of titanium is higher than that of the substrate. In this reaction, titanium species are immediately produced following the dissolution of titanium and spread and re-deposited on the substrate as Na-TNT film, which predominates the dissolving reaction of the substrates. As a result, the surface of the substrate is covered by Na-TNT film, and the dissolution of the substrate was further minimally suppressed. On the other hand, it is considered that when the substrates with ionization tendencies larger than titanium, i.e., substrates such as silicon and tantalum, and titanium were hydrothermally reacted at the same time, the dissolution reaction of substrates predominate the dissolution reaction of titanium. Na-TNT film was not thus obtained on the substrates.

2.3 Hydrogen titanate and anatase-type titanium dioxide nanotube thin films

H^+ ion-exchange treatment for the sodium titanate nanotube thin film and the subsequent calcination can produce an anatase-type titanium dioxide nanotube thin film.

2.3.1 H^+ ion-exchange treatment for sodium titanate nanotube thin films

We performed H^+ ion-exchange treatment for Na-TNT thin film obtained after the 3 h reaction using 0.01 mol/l hydrochloric acid solution at 90 and 140 °C for 3 h. The thin films resulting from treatment at these two temperatures remain attached over the entire surface of each sample. EDX analysis reveal that because the molar ratio of Na/Ti decrease from 0.48 before treatment to 0 after treatment at 90 and 140 °C, Na^+ ions between titanate layers are confirmed to be completely exchanged for H^+ ions. We observe nanotubes with an average outer diameter of 8.3 nm and inner diameter of 3.3 nm in the ion-exchange-treated sample at 90 °C using 0.01 mol/l hydrochloric acid solution (Fig. 6a). No change is observed in the porous structure of the thin film before or after treatment. The XRD pattern for the H^+ ion-exchanged sample at 90 °C shows four diffraction peaks (near 2θ = 9, 24, 29, and 48°) attributed to titanate together with peaks attributed to α-titanium, similar to those for the as-grown sample, as shown in Fig. 7. We therefore believe that the H^+ ion-exchange treatment at 90 °C transforms sodium titanate nanotubes into hydrogen titanate nanotubes while maintaining the crystal structure of titanate, nanotubular morphology, and porous thin-film structure. In contrast, the H^+ ion-exchange treatment at 140 °C replaces the fibrous morphology with rhomboid-shaped particles (average diameter 21 nm) (Fig. 6b) and pores (~ 45 nm diameter) in the interstitial gaps. The XRD pattern of this sample (Fig. 7) shows peaks attributed to anatase. Therefore, a porous thin film consisting of rhomboid-shaped anatase is confirmed to be formed on the titanium metal plate. Change in the crystal structure of sodium titanate nanotubes to anatase nanotubes by acid treatment have been described previously by Tsai et al. (Tsai et al., 2006). They reported that although a nanotube form is maintained by acid treatment at pH 1.6, only irregular-shaped anatase particles are formed by acid treatment at pH 0.38. Zhu et al. (Zhu et al., 2005) reported that hydrogen titanate nanofiber transforms into anatase nanocrystals in dilute (0.05 mol/L) HNO_3 at 80–120 °C. They stated that monodispersed anatase nanocrystals

are obtained at 80 °C and aggregates of nanocrystals are obtained at 120 °C. Our results also suggest that the change in the crystal structure change of titanate compounds to anatase is determined not only by pH but also by the temperature of the ion-exchange treatment. We suggest that the high temperature (140 °C) of the ion-exchange treatment is responsible for the change in the crystal structure of hydrogen titanate to the anatase structure, with a high degree of crystallization, and that this change occurs due to polycondensation and dissolution–redeposition reactions.

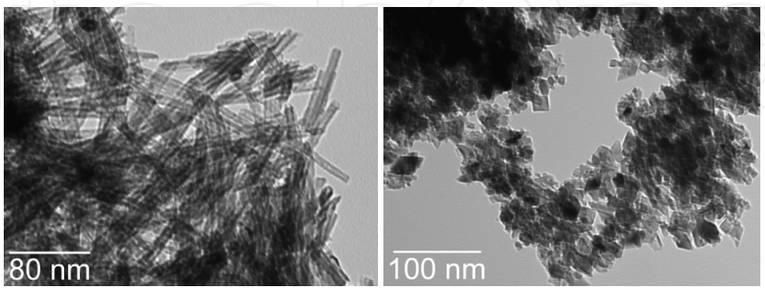

a b

Fig. 6. TEM images of the ion-exchange-treated thin films at 90 °C (a) and 140 °C (b).

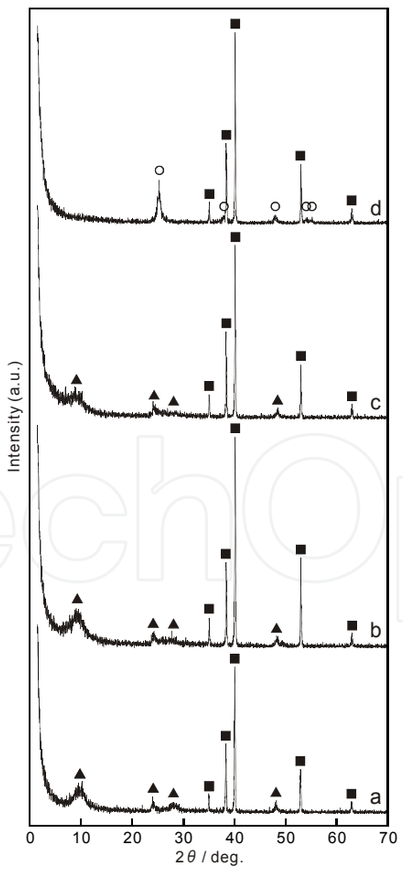

Fig. 7. XRD patterns of the as-grown (a) and the ion-exchange-treated thin films at 40 °C (b), 90 °C (c), and 140 °C (d). Peak assignment: ■, α-titanium; ○, anatase; ▲, titanate.

The temperature required for the complete H^+ ion-exchange reaction would be higher than that previously reported (Kasuga et al., 1998; Kasuga et al., 1999; Tokudome et al., 2004; Uchida et al., 2002; Tokudome et al., 2005; Thorne et al., 2005; Miyauchi et al., 2006; Tokudome et al., 2004; Kasuga et al., 2003), because the H^+ ion-exchange treatments at 40 °C using 0.01, 0.1, and 1 mol/l hydrochloric acid solutions were unsuccessful. H^+ ion-exchange treatment at 40 °C for 3 h using 0.01 and 0.1 mol/l hydrochloric acid solutions resulted in nanotube films respectively. However, substantial amounts of Na^+ ions remained in the samples after treatment. It is considered that elevated temperature assists the diffusion of ions, allowing ion-exchange to occur within the deepest regions of the film. After H^+ ion-exchange treatment at 40 °C using 1.0 mol/l hydrochloric acid solution, the nanotube thin films detached from the titanium metal plate.

2.3.2 Calcination of hydrogen titanate nanotube thin film

The hydrogen titanate nanotube thin films obtained by H^+ ion-exchange treatment at 90 °C using a 0.01 mol/L solution of hydrochloric acid were calcined at 300–900 °C for 3 h in air to transform them into titanium dioxide nanotube thin films. A uniform thin film formed on each sample surface, similar to the sample before calcination.

TEM images (Fig. 8) and XRD patterns (Fig. 9) show that calcination at 300 and 450 °C yields anatase nanotubes. Although the average inner diameter of 3.3 nm for nanotubes synthesized by calcination at 450 °C is similar to that of the as-grown sodium titanate nanotubes, the average outer diameter of the nanotubes decreased from 8.3 nm for the as-grown thin film to 8.1 nm for the anatase nanotubes synthesized by calcination at 450 °C. This slight decrease in the average outer diameter may be due to a phase transition from titanate into anatase. An cross-section image of the thin film calcined at 450 °C is similar to that of the as-grown sodium titanate nanotube thin film. Although a dense phase is observed at the bottom of the thin film (i.e., at the interface between the nanotube phase and the titanium metal), the porous structure composed of fibrous particles is observed in the film itself. Calcination at 600 °C yields anatase nanofibers approximately 11 nm thick, but not nanotubes (Figs. 8c and 9d). The porous structure consisting of fibrous particles are maintained until calcination at 600 °C. Calcination at 750 °C changes the thin film into a porous thin film consisting of particles (with 50-nm average diameter) and interstitial pores (with 79-nm average size) as shown in Fig. 8d. We attribute these changes in morphology to a progressive sintering reaction caused by the high calcination temperature. Furthermore,

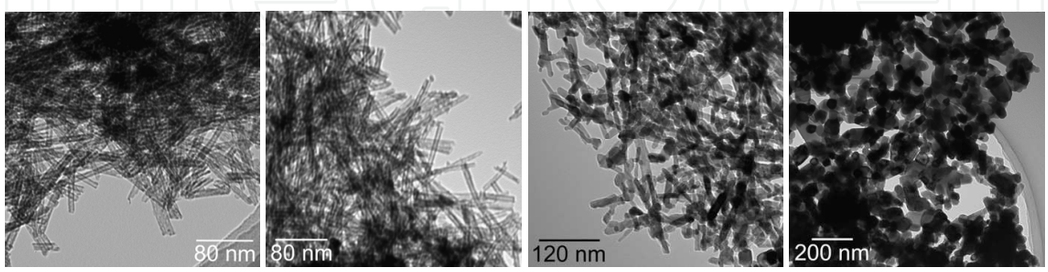

a b c d

Fig. 8. TEM images of the 90 °C ion-exchange-treated thin films calcined at 300 °C (a), 450 °C (b), 600 °C (c), and 750 °C (d).

calcination at 900 °C yields a dense rutile thin film because of the densification and phase transition caused by the sintering of anatase nanoparticles (Fig. 9f).

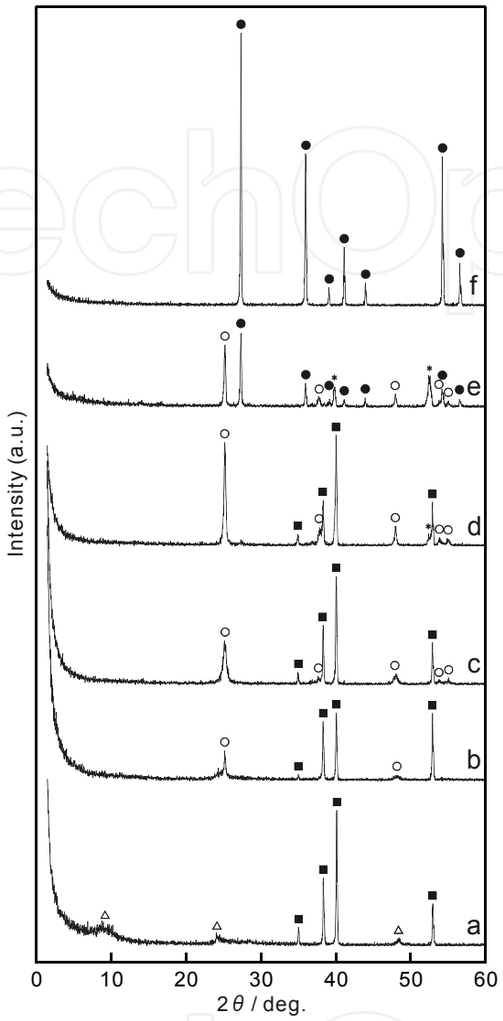

Fig. 9. XRD patterns of the 90 °C ion-exchange-treated (a) and the 90 °C ion-exchange-treated thin films calcined at 300 °C (b), 450 °C (c), 600 °C (d), 750 °C (e), and 900 °C (f). Peak assignment: ■, α-titanium; ○, anatase; ●, rutile; △, hydrogen titanate; *, distorted titanium.

2.4 Silver nanoparticle / silver titanate nanotube nanocomposite thin film

Na-TNT thin film obtained after the 3 h reaction with dimensions of 20 mm × 20 mm × 2 mm (hereafter referred to as Na-TNT-TF) was immersed in 12 mL of 0.05 M silver acetate solution at 40 °C for 3 h, then repeatedly washed with distilled water and dried in a cool dark place, to exchange the Na^+ in the sodium titanate with Ag^+. Hereafter, the sample obtained by the silver ion-exchange treatment of Na-TNT-TF was called Ag-TNT-TF.

The EDX spectra of the samples before and after the silver ion-exchange treatment were then compared. Since the peaks attributed to Na, observed in the samples before the silver ion-

exchange treatment (Na-TNT-TF), disappeared in the samples after the silver ion-exchange treatment (Ag-TNT-TF), and the peaks attributed to Ag appeared after the silver ion-exchange treatment, Na^+ in the sodium titanate seemed to be exchanged with Ag^+ during the silver ion-exchange treatment. However, for the composition calculated from these spectra, the molar ratio of Ag/Ti was 0.67 for Ag-TNT-TF, while the molar ratio of Na/Ti was 0.50 for Na-TNT-TF. This confirmed presence of Ag in an excess compared with the exchangeable cations in the sample. SEM observation at the micrometer scale did not show changes in the morphologies before and after the silver ion-exchange treatment. However, the TEM observations of Ag-TNT-TF (Fig. 10) show particles with sizes ranging from several nanometers to a few dozen nanometers, which were not observable before the ion-exchange treatment. These are considered to be silver nanoparticles, since the color of Ag-TNT-TF was slightly yellow, indicating the formation of silver nanoparticles. The silver nanoparticles were deposited on titanates by the photoreduction of silver ions that were adsorbed on the titanate surface. The excess silver determined through the exchangeable mass of ions observed via EDX analysis is thus attributed to these silver nanoparticles. In other word, in the silver ion-exchange treatment, Ag^+ ion was not only incorporated into the titanate by ion exchange with Na^+ ion, but also deposited on the outer surface of titanate as silver nanoparticles.

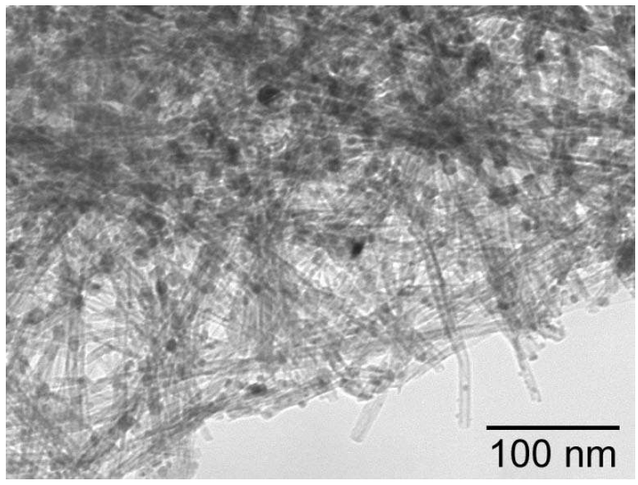

Fig. 10. TEM image of silver nanoparticle/silver titanate nanotube nanocomposite thin film.

Furthermore, TF-XRD patterns of Na-TNT-TF and Ag-TNT-TF shown in Fig. 11 also indicate the transformation of sodium titanate thin film into silver titanate thin film. When silver ion-exchange treatment was performed for Na-TNT-TF, a diffraction peak expressing the interlayer distance of 10 Å that was observed in Na-TNT-TF, disappeared in Ag-TNT-TF. The disappearance of the diffraction peak expressing the interlayer distance of 10 Å is considered to be due to the insertion of Ag^+ ions into an interlayer of titanate and disappearance of the layered structure of titanate. A further reason is a strong and peculiar interaction between the inserted Ag^+ ions and the titanate layer, which would cause a structural change of the layered structure into a three-dimensional structure. This structural change can also be confirmed, as the diffraction peaks in Na-TNT-TF due to the crystal structure of titanate, observed at $2\theta = 24.2°$ and 28.3°, disappeared in Ag-TNT-TF, concomitant with the appearance of a new diffraction peak at $2\theta = 29.3°$ in Ag-TNT-TF. These results indicate the formation of silver titanate nanotube.

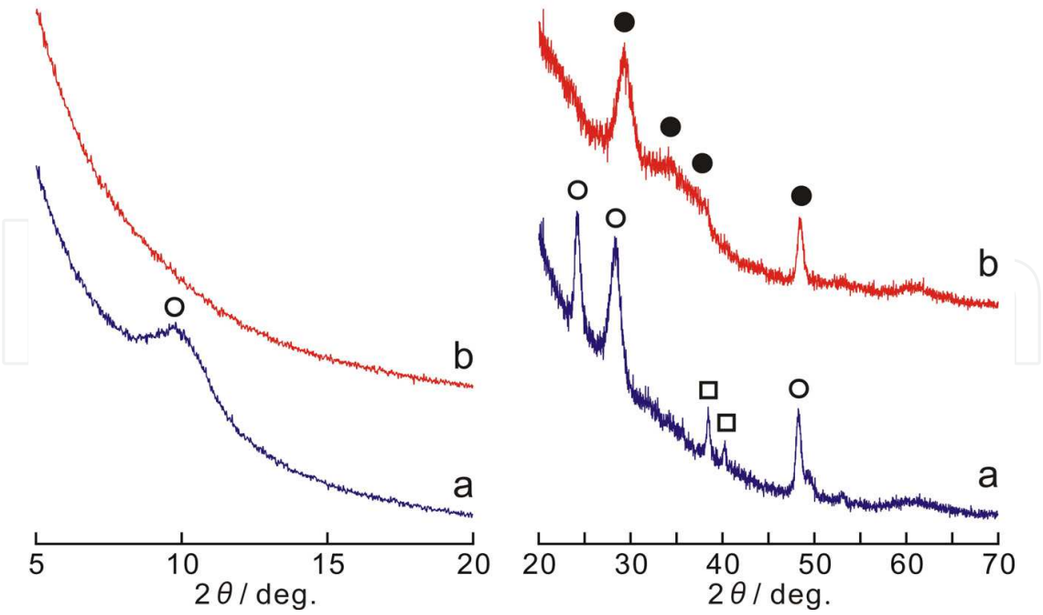

Fig. 11. TF-XRD patterns of sodium titanate nanotube thin film (a) and silver nanoparticle/ silver titanate nanotube nanocomposite thin film (b). Peak assignment: □, titanium; ○, sodium titanate; ●, silver titanate.

3. Antibacterial activities of titanate nanotube thin films

3.1 Elution properties of silver ions from the silver nanoparticle / silver titanate nanotube nanocomposite thin film

The elution properties of silver ions from the samples were examined in various solutions to determine the behavior of silver in MRSA environment or in the body. Ag-TNT-TF with dimensions of 20 mm × 20 mm × 2 mm was immersed in 15 mL physiological saline, phosphate buffered saline (+) (PBS(+)), phosphate buffered saline (−) (PBS(−)), and fetal bovine serum solution, maintained at 37 °C for 24 h. Then, the eluates were collected, centrifuged, and filtrated through a 0.22-μm filter. After filtration, Ag concentration in the eluates was determined by inductively coupled plasma mass spectrometry (ICP-MS). In physiological saline, PBS(+), and PBS(−), almost the same average concentration of eluted silver was measured—300, 320, and 440 ppb, respectively. The eluted silver ions may originate from metallic silver and silver titanate. Since the solubility of metallic silver is known to be very small, the large portion of eluted silver was eluted by exchanging silver ions in titanates with Na^+, K^+, and H^+ in the solutions. On the other hand, in fetal bovine serum, the average eluted silver concentration was measured in large amounts—82000 ppb for Ag-TNT-TF. This was because a large quantity of a compound composed of silver and a protein was formed together with AgCl, since the protein that exists in fetal bovine serum has very high affinity with Ag^+ through the –SH group or –NH group in the protein, and the amount of exchangeable cations in fetal bovine serum was larger than that in physiological saline and PBS. Moreover, when the silver elution test in fetal bovine serum was performed for a silver metal plate under similar conditions as that for Ag-TNT-TF, silver of 7900 ppb was eluted. This amount was also significantly smaller than that for of Ag-TNT-TF. In the

silver elution test of Ag-TNT-TF, although silver is eluted from silver nanoparticles deposited on the surface of titanate, its elution amount is thus considered small. Consequently, in the XRD and TF-XRD patterns of the sample obtained by the silver elution test of Ag-TNT-TF, diffraction peaks appeared near $2\theta = 10°$, 24° and 28°, which were not observed in Ag-TNT-TF. These diffraction peaks of the sample obtained by the silver elution test of Ag-TNT-TF appeared at the same locations as the diffraction peaks observed in Na-TNT-TF. This indicates that the crystal structure of the sample obtained by the silver elution test of Ag-TNT-TF is similar to that of Na-TNT-TF. The likely reasons are as follows: (1) the layered structure of titanate of Na-TNT-TF transformed into a three-dimensional structure because Ag^+ ions were inserted into the interlayer of titanate by the silver ion-exchange treatment to form silver titanate, (2) Ag^+ ions were eluted from the silver titanate and Na^+ ions were reinserted into the titanate during the silver elution test; and (3) the three-dimensional structure of titanate returned to the original condition as in Na-TNT-TF. Thus, it is clearly demonstrated that insertion (intercalation) and elimination (deintercalation) of Ag^+ ions occurs during the silver ion-exchange treatment and the silver elution test, respectively. Therefore, this experiment indicated that Ag^+ ions in silver titanate greatly contributed to the elution of Ag^+. Diffraction peaks attributable to AgCl were also observed in the sample obtained by the silver elution test of Ag-TNT-TF, because AgCl particles were formed by the reaction between eluted Ag^+ and Cl^- in fetal bovine serum. Since fetal bovine serum solution is considered as the system most similar to MRSA environment, silver elution tests in fetal bovine serum solution were repeated (Fig. 12). In Ag-TNT-TF, the elution concentration slowly decreased from 94000 ppb for the first test to 11000 ppb for the tenth, indicating that a large amount of eluted silver was measured in the tenth test for Ag-TNT-TF. The 2-step elution curve was obtained from Ag-TNT-TF. A rapid elution of a large amount of silver at the initial stage of the repeated elution test (between the first and third time) was considered to be mainly due to Ag^+ ion elution from the silver titanate based on the ion-exchange reaction. Since the elution reaction (ion-exchange reaction) of Ag^+ from silver titanate is rapid, the elution of Ag^+ is considered to be almost completed at the initial stage of the repeated elution test. These discussions are also supported by the above described TF-XRD data, indicating that crystal structure of the sample obtained by the silver elution test of Ag-TNT-TF is similar to that of Na-TNT-TF. Therefore, a slow elution of a small amount of silver after the forth repetition of the elution test was considered to be mainly because of silver elution from the silver nanoparticles. This two-step elution curve is difficult to explain if it is considered that only silver nanoparticles are formed in the thin film, but it is reasonably explained if two types of Ag (silver nanoparticles and silver titanate) exhibiting different elution behaviors are present in Ag-TNT-TF. The silver titanates loading silver nanoparticles would be promising as a novel antibacterial material, because they have two silver sources. The silver-ion elution property of silver titanate would be different from that of the silver nanoparticles, i.e., the elution speed of silver ions from silver titanate would be greater than that from silver nanoparticles. Therefore, silver titanate would be effective for short-term bacterial killing, and silver nanoparticles would be effective for long-term antibacterial action. Since we have already found that a thicker (i.e., 20 μm thick) titanate nanotube film can be formed after a longer reaction time or 20 h in NaOH solution, it would be possible to prolong the elution period of silver ions and to increase the amount of eluted silver ions or the duration.

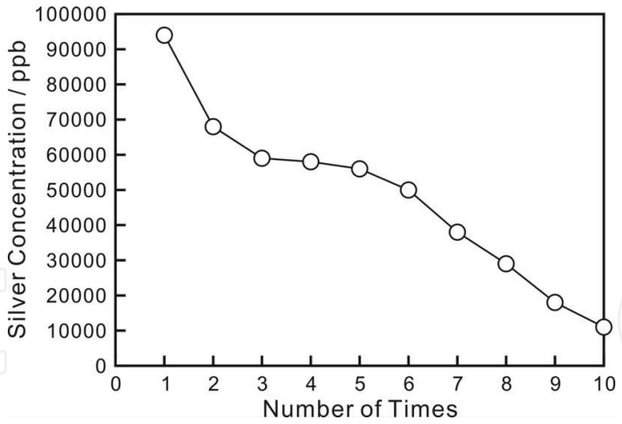

Fig. 12. Repeated silver ion elution test of silver nanoparticle/silver titanate nanotube nanocomposite thin film.

3.2 Antibacterial property of silver nanoparticle / silver titanate nanotube nanocomposite thin film

The modified Japanese Industrial Standard test (JIS Z 2801) was performed as an antibacterial test as follows. To approximate an infection environment within an actual organism, an inactivated bovine serum (0.4 mL) was used as a solvent of bacterial suspension to create a eutrophic condition, and the antibacterial test was conducted using MRSA with a biofilm-forming gene. A bacterial suspension (0.4 mL) was dropped on a 50 mm × 50 mm × 2 mm test piece, covered with a 40 mm × 40 mm polyethylene film (Elmex Corp.), and cultured at 37 °C for 24 h. The test piece was washed, and the viable MRSA count was determined. The antibacterial test was performed thrice for each of the samples of Na-TNT-TF and Ag-TNT-TF, to obtain averaged values of viable MRSA counts. The antibacterial activity value (R) for the sample was calculated as follows.

$$R = \{\log(B/A) - \log(C/A)\} = \log(B/C)$$

Here, A, B, and C are the average viable MRSA counts just after inoculation, after 24 h for a blank and after 24 h for a sample, respectively. The viable MRSA count just after the inoculation was 2.1×10^5 CFU/sample, and for a blank, the average viable MRSA count after 24 h increased to 5.9×10^8 CFU/sample. In Na-TNT-TF, the average viable MRSA count after 24 h was slightly less than that of the blank: 1.1×10^7 CFU/sample. On the other hand, in Ag-TNT-TF, the average viable MRSA count after 24 h was markedly small: 3.3×10^2 CFU/sample. R increased from 1.7 for Na-TNT-TF to 6.3 for Ag-TNT-TF through the silver ion-exchange treatment. These results indicate that the silver ion-exchanged titanate thin films display high antibacterial activity against MRSA. It was also revealed that although the crystal structure of titanate itself does not have a large antibacterial effect, higher antibacterial activity arises in the silver in the titanate. The conversion of sodium titanates into antibacterial materials through the silver ion-exchange treatment can apply to other nanostructured sodium titanates. For example, by the same silver ion-exchange treatment, porous sodium titanate film calcined at 600 °C reported by Kim et al. (Kim et al., 1997) can also be converted into silver nanoparticle / silver titanate nanocomposite thin film with high antibacterial activity for MRSA of R=6.7.

4. Apatite-forming ability of titanate and titanium dioxide nanotube thin films

The three thin films (Na-TNT-TF, TiO_2-NT-FT (anatase type titanium dioxide nanotube thin film formed by the H^+ ion-exchange treatment and calcination at 450 °C of Na-TNT-TF), Ag-TNT-TF) formed on a titanium metal were immersed in simulated body fluid (SBF) and monitored the development of apatite formation on their surfaces. In accordance with ISO 23317, "Implants for surgery-*In vitro* evaluation for apatite-forming ability of implant materials," we evaluated the apatite-forming ability on the surface of the coating in SBF. A plate was placed in 96.0 mL SBF at 36.5°C. After 2, 4, and 14 days, the plate was removed and gently rinsed with water. The surface of the plate was dried in air.

For Na-TNT-TF, after immersing the film for 4 days, the SEM images showed only nanotubes and no substances with foliaceous morphology peculiar to apatite; the XRD patterns remained unchanged. However, when the SBF immersion was extended to 14 days, the SEM images showed the surface of the film to be completely covered with a dome-shaped form consisting of foliaceous particles peculiar to apatite (Figs. 13a, b); the XRD pattern showed diffraction peaks attributable to apatite. Thus, apatite is confirmed to be formed on the sodium titanate thin films. In addition, after immersing the hydrogen titanate nanotube thin film formed by exchanging Na^+ ions between the layers of the layered sodium titanate for H^+ ions in SBF for 4 days, no apatite was evident. This lack of apatite indicates that ions (Na^+ and H^+) between the titanate layers do not particularly contribute to the acceleration of the apatite formation. In contrast, for TiO_2-NT-FT formed by the 450°C calcination of the hydrogen titanate nanotube thin film and Ag-TNT-TF, after immersing the

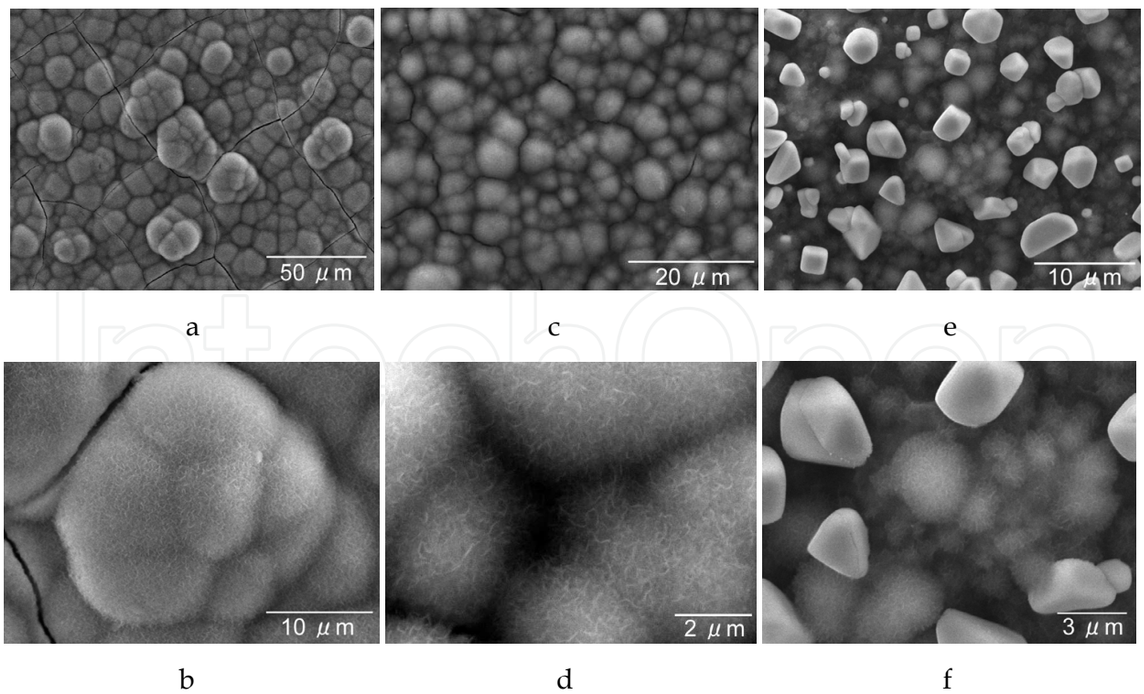

Fig. 13. Low magnification (a, c, e) and high magnification (b, d, f) SEM images of Na-TNT-TF (a, b), TiO_2-NT-FT (c, d), and Ag-TNT-TF (e, f) after immersions in SBF.

films for 4 days, the SEM images showed a stretch of the dome-shaped form consisting of foliaceous particles peculiar to apatite (Figs. 13c, d). XRD patterns of the two films showed diffraction peaks attributable to apatite, respectively. These results indicate that the surfaces of these two thin films are completely covered with apatite and that the apatite-forming ability of the two films is greater than that of Na-TNT-TF having layered structure. In contrast, for TiO_2-NT-FT after immersing the film in SBF for 2 days, the surface is thinly covered with apatite. However immersing Ag-TNT-TF for 2 days, the surface is almost covered with a dome-shaped form consisting of foliaceous particles peculiar to the apatite (Figs. 13e, f). The apatite-forming ability of Ag-TNT-TF is, thus, slightly higher than that of TiO_2-NT-FT.

We then investigated the newly observed high apatite-forming ability of silver nanoparticle/silver titanate nanocomposite thin film (Ag-TNT-TF). After immersing the film in SBF for 4 days, we observed bulky particles of a few micrometers in diameter together with apatite. XRD pattern shows diffraction peaks attributable to silver chloride. EDX element mapping analysis shows the bulky particles to be composed of Ag and Cl (Fig. 14) and, therefore, to be silver chloride particles. Therefore, Ag^+ ions are eluted from silver titanate mainly by ion-exchange reaction with cations, resulting in deposition of silver chloride particles. After immersing the film in SBF for 1 day, SEM images reveal only bulky AgCl particles on the film surface, however immersing the film for 2 days, the surface is almost covered with a dome-shaped form consisting of foliaceous particles peculiar to the apatite (Figs. 13e, f), as mentioned above. We clarified whether silver nanoparticle or silver titanate contributes more to the apatite formation by investigating the apatite-forming ability of a silver metal plate. After immersing the plate in SBF for 4 days, no apatite formation was evident; thus, the silver titanate nanotubes are responsible for the high apatite-forming ability. Researchers have reported that the effects of crystal structure (Uchida et al., 2003) and surface hydroxyl groups such as Ti-OH (Kasuga et al., 2002) influence the apatite formation on the titanium compounds immersed in SBF. Kokubo et al. reported that the apatite-forming ability is improved by the crystal structure transformation of sodium titanate into titanium dioxide (Fujibayashi et al., 2001; Uchida et al., 2002; Takemoto et al., 2006). Although the detailed crystal structure of silver titanate is not yet known, we speculate that the surface atomic arrangement and surface functional groups of silver titanate might be suitable for rapid apatite formation. We further investigated the high apatite forming ability by considering –OH groups that influence apatite formation using the FT-IR measurements. As shown in Fig. 15, Na-TNT-TF and TiO_2-NT-FT exhibited similar absorption spectra in a wide range of 3000−3700 cm^{-1}. These absorption spectra are considered to be mainly due to water molecules adsorbed on the inner and outer surfaces of nanotubes and partially due to –OH groups on the surface. Unlike Na-TNT-TF and TiO_2-NT-FT, strong absorption was observed at 3000−3400 cm^{-1} in addition to 3400−3700 cm^{-1} in Ag-TNT-TF. This absorption at 3000−3400 cm^{-1} is considered to indicate the existence of surface –OH groups due to silver titanate. A surface atomic arrangement peculiar to silver titanate would arise and a large number of –OH groups would be generated on the nanotube surfaces, which would stimulate apatite formation.

Oh et al. (Oh et al., 2005) and Tsuchiya et al. (Tsuchiya et al., 2006) reported anatase-type titanium dioxide nanotube thin films synthesized by anodization and heat treatment of the titanium metal. We compared the apatite-forming ability of these nanotube thin films with

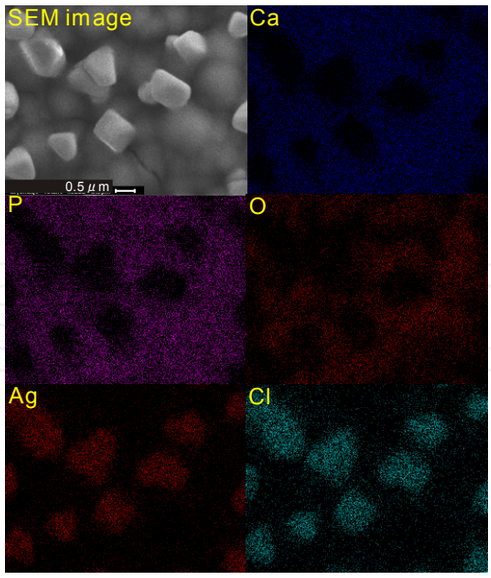

Fig. 14. Elemental mapping performed on Ag-TNT-TF after immersion in SBF for 4 days using EDX analysis.

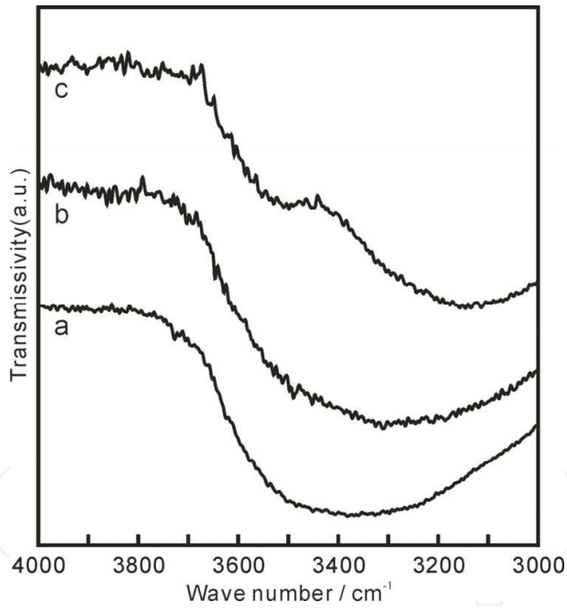

Fig. 15. FT-IR spectra of Na-TNT-TF (a), TiO_2-NT-FT (b), and Ag-TNT-TF (c).

that of TiO_2-NT-FT obtained in this study by immersing the film in SBF for 2 days. SEM images show not only a small amount of the dome-shaped form consisting of foliaceous particles peculiar to apatite, but also several slightly swelled and whitish areas. EDX element mapping on this thin film revealed that titanium dioxide nanotubes exist in the blackish areas and apatite exists in the whitish areas. At this point, after 2 days of immersion, the apatite phase has grown slightly but not yet achieved its dome-shaped form. Therefore, the apatite-forming ability of TiO_2-NT-FT is slightly superior though still similar

to that of the thin film with 2-μm long nanotube synthesized by Tsuchiya et al. (Tsuchiya et al., 2006) and clearly superior to that of the nanotube thin film synthesized by Oh et al. (Oh et al., 2005) and the thin film with 500-nm long nanotube synthesized by Tsuchiya et al. (Tsuchiya et al., 2006). While comparing the ratio of the void parts to the anatase-type titanium dioxide part on the surface using SEM images, we found the proportion consisting anatase-type titanium dioxide to be larger in the surface of our synthesized thin film as compared to that in the surfaces of the thin films reported by Oh et al. and Tsuchiya et al. Hence, the apatite-forming ability of our film is also correspondingly higher.

5. Conclusion

In this study, novel procedure of synthesis and fixation of Na-TNT onto titanium metals with various morphologies such as plate, wire, mesh, tube, and sphere was reported. Especially, since the Na-TNT/Ti composite wires have softness and flexibility peculiar to metal titanium because of the existence of titanium metal in its core part, this wire can be fabricated into various shapes of cloth, fiber, etc. with centimeter or meter size by using conventional spinning techniques. The Na-TNT thin films can be transformed into anatase-type titanium dioxide nanotube thin films. Another advantage of the proposed procedure is that the thickness of the thin films produced is greater than that of the thin films reported by other researchers. Therefore, Na-TNT's applications mentioned in the introduction would be remarkably expanded. In addition, the novel growth of the Na-TNT film on substrates such as Co–Cr alloy and SUS316L and simple patterning of the Na-TNT phase by the hydrothermal transcription method were also reported. As these substrates including titanium metal, Co-Cr alloy, and SUS316L have superior mechanical properties and corrosion resistance, they are frequently used as implants such as artificial joints. Generally, the coating of films to implants with complex shapes requires thin films with uniform and controlled thickness, and a high fixing strength to the implants. Because of the direct growth of the nanotubes from the substrate, our proposed method is very simple and the fixing strength to the substrate is expected to be higher. Therefore, the method proposed in the present study has excellent potential for these biomedical applications.

Next, through a silver ion-exchange treatment, Na^+ ions in sodium titanate nanotube were exchanged with Ag^+ ions in silver acetate solution, along with the loading of silver nanoparticles on the titanate surfaces, and the layered structure of titanate transformed into a new three-dimensional crystal structure. Results of silver ion elution tests of the obtained thin films in fetal bovine serum solution indicate that the release period and the number of silver ions released from the silver titanate thin films can be controlled. The silver ion-exchanged titanate thin films showed high antibacterial activity against MRSA. It was also revealed that although the crystal structure of titanate itself has no large antibacterial effect, higher antibacterial activity mainly arises from the silver ions held in the titanate. The samples coated with apatite containing silver and silver plate have already been reported as possessing antibacterial properties through metallic silver with low solubility. In contrast, in this study, the antibacterial properties were mainly caused by the elution of silver ions from a titanate with an ion-exchange property. Since the thin film obtained by this study has a higher silver-ion elution speed, greater and more rapid antibacterial effects than in metallic silver can be expected. Since we have also revealed that the morphology, thickness, and crystal structure of the titanate phase can be controlled, we think that this can also promise

control of the antibacterial properties, i.e., the duration and amount of antibacterial activity, for the future. The obtained results should aid the development of more convenient and inexpensive antibacterial implants.

Furthermore, the present study compares the apatite-forming ability of a sodium titanate nanotube thin film, an anatase-type titanium dioxide nanotube thin film, and a silver nanoparticle/silver titanate nanotube nanocomposite thin film. Of these, the apatite-forming ability of the silver titanate nanotube was higher than that of the titanium dioxide nanotubes or the sodium titanate nanotubes, in that order. This superior apatite-forming ability of the silver nanoparticle/silver titanate nanotube nanocomposite thin film is a novel phenomenon and is presumably due to the surface atomic arrangement of silver titanate, the large amount of Ti-OH formed on the nanotube surface, or both. In conclusion, the silver nanoparticle/silver titanate nanotube nanocomposite thin film, which have the antibacterial property and the ability to form bone-like apatite, i.e., the osteoconductive property, may have bright prospects for future use in implant materials such as artificial joints.

6. Acknowledgment

This research was partially supported by KAKENHI (16685021, 19750172) and Saga University Dean's Grant 2010 For Promising Young Researchers. Figures are reproduced with permission from American Chemical Society, Elsevier, and John Wiley & Sons.

7. References

Alt, V.; Bitschnau, A.; Österling, J.; Sewing, A.; Meyer, C.; Kraus, R.; Meissner, S. A.; Wenisch, S.; Domann, E. & Schnettler, R. (2006). The effects of combined gentamicin–hydroxyapatite coating for cementless joint prostheses on the reduction of infection rates in a rabbit infection prophylaxis model. *Biomaterials*, Vol. 27, pp. 4627-4634.

Bavykin, D. V.; Lapkin, A. A.; Plucinski, P. K.; Friedrich, J. M. & Walsh, F. C. (2005). Reversible storage of molecular hydrogen by sorption into multilayered TiO_2 nanotubes. *The Journal of Physical Chemistry B*, Vol. 109, pp. 19422-19427.

Bavykin, D. V.; Friedrich, J. M. & Walsh, F. C. (2006). Protonated Titanates and TiO_2 Nanostructured Materials: Synthesis, Properties, and Applications. *Advanced Materials*, Vol. 18, pp. 2807-2824.

Byon, E.; Jeong, Y.; Takeuchi, A.; Kamitakahara, M. & Ohtsuki, C. (2007). Apatite-forming ability of micro-arc plasma oxidized layer of titanium in simulated body fluids. *Surface and Coat Technology*, Vol. 201. pp. 5651-5654.

Chen, Q.; Zhou, W.; Du, G. & Peng, L.-M. (2002). Trititanate nanotubes made via a single alkali treatment. *Advanced Materials*, Vol. 14, pp. 1208-1211.

Chen, W.; Liu, Y.; Courtney, H. S.; Bettenga, M.; Agrawal, C. M.; Bumgardner, J. D. & Ong, J. L. (2006). In vitro anti-bacterial and biological properties of magnetron co-sputtered silver-containing hydroxyapatite coating. *Biomaterials*, Vol. 27, pp. 5512-5517.

Chi, B.; Victorio, E. S. & Jin, T. (2007). Synthesis of TiO_2-Based Nanotube on Ti Substrate by Hydrothermal Treatment. *Journal of Nanoscience and Nanotechnology*, Vol. 7, pp. 668-672.

Fujibayahsi, S.; Nakamura, T.; Nishiguchi, S.; Tamura, J.; Uchida, M.; Kim, H. M. & Kokubo, T. (2001). Bioactive titanium : effect of sodium removal on the bone-bonding ability of bioactive titanium prepared by alkali and heat treatment. *Journal of Biomedical Materials Research*, Vol. 56, pp. 562-570.

Guo, Y.; Lee, N.-H.; Oh, H.-G.; Yoon, C.-R.; Park, K.-S.; Lee, H.-G.; Lee, K.-S. & Kim, S.-J. (2007). Structure-tunable synthesis of titanate nanotube thin films via a simple hydrothermal process. *Nanotechnology*, Vol. 18, pp. 295608-295616.

Hanawa, T.; Kon, M.; Ukai, H.; Murakami, K.; Miyamoto, Y. & Asaoka, K. (1997). Surface Modification of Titanium in Calcium-Ion-Containing Solutions. *Journal of Biomedical Materials Research*, Vol. 34, pp. 273-278.

Hamada, K.; Kon, M.; Hanawa, T.; Yokoyama, K.; Miyamoto, Y. & Asaoka, K. (2002). Hydrothermal modification of titanium surface in calcium solutions. *Biomaterials*, Vol. 23, pp. 2265-2272.

Hardes, J.; Ahrens, H.; Gebert, C.; Streitbuerger, A.; Buerger, H.; Erren, M.; Gunsel, A.; Wedemeyer, C.; Saxler, G & Winkelmann, W. (2007). Lack of toxicological side-effects in silver-coated megaprostheses in humans. *Biomaterials*, Vol. 28, pp. 2869-2875.

Imai, H.; Takei, Y.; Shimizu, K.; Matsuda, M. & Hirashima, H. (1999). Direct preparation of anatase TiO_2 nanotubes in porous alumina membranes. *Journal of Materials Chemistry*, Vol. 9, pp. 2971-2972.

Inoue, Y.; Noda, I.; Torikai, T.; Watari, T.; Hotokebuchi, T. & Yada, M. (2010). TiO_2 nanotube, nanowire, and rhomboid-shaped particle thin films fixed on a titanium metal plate. *Journal of Solid State Chemistry*, Vol. 183, pp. 57-64.

Inoue, Y.; Uota, M.; Torikai, T.; Watari, T.; Noda, I.; Hotokebuchi, T. & Yada, M. (2010). Antibacterial properties of nanostructured silver titanate thin films formed on a titanium plate, *Journal of Biomedical Materials Research Part A*, Vol. 92A, pp. 1171-1180.

Jiang, Z.; Yang, F.; Luo, N.; Chu, B. T. T.; Sun, D.; Shi, H.; Xiao, T. & Edwards, P. P. (2008). Solvothermal synthesis of N-doped TiO_2nanotubes for visible-light-responsive photocatalysis. *Chemical Communication*, pp. 6372-6374.

Jung, J. H.; Kobayashi, H.; van Bommel, K. J. C.; Shinkai, S. & Shimizu, T. (2002). Creation of Novel Helical Ribbon and Double-Layered Nanotube TiO_2 Structures Using an Organogel Template. *Chemistry of Materials*, Vol. 14, pp. 1445-1447.

Jonášová, L.; Müller, F. A.; Helebrant, A.; Strnad, J. & Greil, P. (2003). Biomimetic apatite formation on chemically treated titanium. *Biomaterials*, Vol. 25, pp. 1187-1194.

Kasuga, T.; Hiramatsu, M.; Hoson, A.; Sekino, T. & Niihara, K. (1998). Formation of titanium oxide nanotube. *Langmuir*, Vol. 14, pp. 3160-3163.

Kasuga, T.; Hiramatsu, M.; Hoson, A.; Sekino, T. & Niihara, K. (1999). Titania nanotubes prepared by chemical processing. *Advanced Materials*, Vol. 11, pp. 1307-1311.

Kasuga, T.; Kondo, H. & Nogami, M. (2002). Apatite formation on TiO_2 in simulated body fluid. *Journal of Crystal Growth*, Vol. 235, pp. 235-240.

Kasuga, T. (2003). *Jpn. Kokai Tokkyo Koho*, P2003-220127A.

Kim, G.-S.; Ansari, S. G.; Seo, H.-K.; Kim, Y.-S. & Shin, H.-S. (2007). Effect of annealing temperature on structural and bonded states of titanate nanotube films. *Journal of Applied Physics*, Vol. 101, pp. 024314-024320.

Kim, H. M.; Miyaji, F.; Kokubo, T. & Nakamura, T. (1996). Preparation of bioactive Ti and its alloys via simple chemical surface treatment. *Journal of Biomedical Materials Research*, Vol. 32, pp. 409-417.

Kim, H. M.; Miyaji, F.; Kokubo, T. & Nakamura, T. (1997). Effect of heat treatment on apatite-forming ability of Ti metal induced by alkali treatment. *Journal of Materials Science: Materials in Medicine*, Vol. 8, pp. 341-347.

Kim, H. M.; Miyaji, F.; Kokubo, T.; Nishiguchi, S. & Nakamura, T. (1997). Graded surface structure of bioactive titanium prepared by chemical treatment. *Journal of Biomedical Materials Research*, Vol. 45, pp. 100-107.

Kim, H. M.; Himeno, T.; Kawashita, M.; Lee, J. H. & Kokubo, T. (2003). Surface Potential Change in Bioactive Titanium Metal during the Process of Apatite Formation in Simulated Body Fluid. *Journal of Biomedical Materials Research Part A*, Vol. 67A, pp. 1305-1309.

Kokubo, T.; Miyaji, F.; Kim, H. M. & Nakamura, T. (1996). Spontaneous Formation of Bonelike Apatite Layer on Chemically Treated Titanium Metals. *Journal of the American Ceramic Society*, Vol. 79, pp. 1127-1129.

Kokubo, T. & Takadama, H. (2006). How useful is SBF inpredicting in vivo bone bioactivity ? *Biomaterials*, Vol. 27, pp. 2907-2915.

Kon, M.; Sultana, R.; Fujihara, E.; Asaoka, K. & Ichikawa, T. (2007). Hydroxyapaite Morphology Control by Hydrothermal Treatment. *Key Engineering Materials*, Vol. 330-332, pp. 737-740.

Kubota, S.; Johkura, K.; Asanuma, K.; Okouchi, Y.; Ogiwara, N.; Sasaki, K. & Kasuga, T. (2004). Titanium oxide nanotubes for bone regeneration. *Journal of Materials Science: Materials in Medicine*, Vol. 15, pp. 1031-1035.

Ma, R.; Bando, Y. & Sasaki, T. (2003). Nanotubes of lepidocrocite titanates. *Chemical Physics Letters*, Vol. 380, pp.577-582.

Ma, R.; Sasaki, T. & Bando, Y. (2004). Layer-by-Layer Assembled Multilayer Films of Titanate Nanotubes, Ag- or Au-Loaded Nanotubes, and Nanotubes/Nanosheets with Polycations. *Journal of the American Chemical Society*, Vol. 126, pp. 10382-10388.

Macak, J. M.; Tsuchiya, H. & Schmuki, P. (2005). High-Aspect-Ratio TiO_2 Nanotubes by Anodization of Titania. *Angewandte Chemie International Edition*, Vol. 44, pp. 2100-2102.

Miyauchi, M.; Tokudome, H. Toda, Y.; Kamiya, T. & Hosono, H. (2006). Electron Field Emission from TiO_2 Nanotube Arrays Synthesized by Hydrothermal Reaction. *Applied Physics Letters*, Vol. 89, pp.043114-043116.

Muramatsu, K.; Uchida, M.; Kim, H. M.; Fujisawa, A. & Kokubo, T. (2003). Thromboresistance of alkali- and heat-treated titanium metal formed with apatite. *Journal of Biomedical Materials Research Part A*, Vol. 65A, pp. 409-416.

Nakagawa, M.; Zhang, L.; Udou, K.; Matsuya, S. & Ishikawa, K. (2005). Effects of hydrothermal treatment with $CaCl_2$ solution on surface property and cell response of titanium implants. *Journal of Materials Science: Materials in Medicine*, Vol. 16, pp. 985-991.

Nakahira, A.; Kato, W.; Tamai, M.; Isshiki, T.; Nishio, K. & Aritani, H. (2004). Synthesis of nanotube from a layered $H_2Ti_4O_9H_2O$ in a hydrothermal treatment using various titania sources. *Journal of Materials Science*, Vol. 39, pp. 4239-4245.

Nishiguchi, S.; Nakamura, T.; Kobayashi, M.; Kim, H. M.; Miyaji, F. & Kokubo, T. (1999). The effect of heat treatment on bone-bonding ability of alkali-treated titanium. *Biomaterials*, Vol. 20, pp. 491-500.

Oh, S. H.; Finõnes, R. R.; Daraio, C.; Chen, L. H. & Jin, S. (2005). Growth of nano-scale hydroxyapatite using chemically treated titanium oxide nanotubes. *Biomaterials*, Vol. 26, pp. 4938-4943.

Ohtsu, N.; Abe, C.; Ashino, T.; Semboshi, S. & Wagatsuma, K. (2008). Calcium-hydroxide slurry processing for bioactive calcium-titanate coating on titanium. *Surface and Coat Technology*, Vol. 202, pp. 5110-5115.

Ohtsuki, C.; Iida, H.; Hayakawa, S. & Osaka, A. (1997). Bioactivity of titanium treated with hydrogen peroxide solutions containing metal chlorides. *Journal of Biomedical Materials Research*, Vol. 35, pp. 39-47.

Shin, H.; Jeong, D.-K.; Lee, K.; Sung, M. M. & Kim, J. (2004). Formation of TiO_2 and ZrO_2 Nanotubes Using Atomic Layer Deposition with Ultra-Precise Wall Thickness Control, *Advanced Materials*, Vol. 16, pp. 1197-1200.

Sun, X. & Li, Y. (2003). Synthesis and Characterization of Ion-Exchangeable Titanate Nanotubes. *Chemistry - A European Journal*, Vol. 9, pp. 2229-2238.

Tsai, C.-C. & Teng, H. (2006). Structural features of nanotubes synthesized from NaOH treatment on TiO_2 with different post-treatments. *Chemistry of Materials*, Vol. 18, pp. 367-373.

Takemoto, M.; Fujibayashi, S.; Neo, M.; Suzuki, J.; Matsushita, T.; Kokubo, T. & Nakamura, T. (2006). Effect of sodium removal by dilute HCl treatment. *Biomaterials*, Vol. 27, pp. 2682-2691.

Thorne, A.; Kruth, A.; Tunstall, D.; Irvine, J. T. S. & Zhou, W. (2005). Formation, Structure, and Stability of Titanate Nanotubes and their Proton Conductivity. *The Journal of Physical Chemistry B*, Vol. 109, pp. 5439-5444.

Tian, Z. R.; Voigt, J. A.; Liu, J.; Mckenzie, B. & Xu, H. (2003). Large oriented arrays and continuous films of TiO_2-based nanotubes. *Journal of the American Chemical Society*, Vol. 125, pp. 12384-12385.

Tokudome, H. & Miyauchi, M. (2004). N-doped TiO_2 Nanotube with Visible Light Activity. *Chemistry Letter*, Vol. 33, pp. 1108-1109.

Tokudome, H. & Miyauchi, M. (2004). Titanate nanotube thin films via alternate layer deposition. *Chemical Communication*, pp. 958-959.

Tokudome, H. & Miyauchi, M. (2005). Electrochromism of titanate-based nanotubes. *Angewandte Chemie International Edition*, Vol. 44, pp. 1974-1977.

Tsuchiya, H.; Macak, J. M.; Müller, L.; Kunze, J.; Müller, F.; Greil, P.; Virtanen, S. & Schmuki, P. (2006). Hydroxyapatite growth on anodic TiO_2 nanotubes. *Journal of Biomedical Materials Research Part A*, Vol. 77A, pp. 534-541.

Uchida, S.; Chiba, R.; Tomiha, M.; Masaki, N. & Shirai, M. (2002). Application of Titania Nanotubes to a Dye-Sensitized Solar Cell. *Electrochemistry*, Vol. 70, pp. 418-420.

Uchida, M.; Kim, H. M.; Kokubo, T.; Fujibayashi, S. & Nakamura, T. (2002). Effect of water treatment on the apatite-forming ability of NaOH-treated titanium metal. *Journal of Biomedical Materials Research*, Vol. 63, pp. 522-530.

Uchida, M.; Kim, H. M.; Kokubo, T.; Fujibayashi, S. & Nakamura, T. (2003). Structural dependence of apatite formation on titania gels in a simulated body fluid. *Journal of Biomedical Materials Research Part A*, Vol. 64A, pp. 164-70.

Wang, F.; Liao, Y.; Wang, M.; Gong, P.; Li, X.; Tang, H.; Man, Y.; Yuan, Q.; Wei, N.; Tan, Z. & Ban, Y. (2007). Evaluation of Sodium Titanate Coating on Titanium by Sol-Gel Method In Vitro. *Key Engineering Materials*, Vol. 330-332, pp. 777-780.

Wang, X. J.; Li, Y. C.; Lin, J. G.; Yamada, Y.; Hodgson, P. D. & Wen, C. E. (2008). In vitro bioactivity evaluation of titanium and niobium metals with different surface morphologies. *Acta Biomaterialia*, Vol. 4, pp. 1530-1535.

Wang, X. X.; Hayakawa, S.; Tsuru, K. & Osaka, A. (2001). A comparative study of in vitro apatite deposition on heat-, H_2O_2-, and NaOH- treated titanium surfaces. *Journal of Biomedical Materials Research*, Vol. 54, pp. 172-178.

Wang, X. X.; Yan, W.; Hayakawa, S.; Tsuru, K. & Osaka, A. (2003). Apatite deposition on thermally and anodically oxidized titanium surfaces in a simulated body fluid. *Biomaterials*, Vol. 24, pp. 4631-4637.

Wu, D.; Liu, J.; Zhao, X.; Li, A.; Chen, Y. & Ming, N. (2006). Sequence of events for the formation of titanate nanotubes, nanofibers, nanowires, and nanobelts. *Chemistry of Materials*, Vol. 18, pp. 547-553.

Xiong, J.; Li, Y.; Hodgson, P. D. & Wen, V. (2010). Nanohydroxyapatite coating on a titanium–niobium alloy by a hydrothermal process. *Acta Biomaterialia*, Vol. 6, pp. 1584-1590.

Yada, M.; Inoue, Y.; Uota, M.; Torikai, T.; Watari, T.; Noda, I. & Hotokebuchi, T. (2007). Plate, Wire, Mesh, Microsphere, and Microtube Composed of Sodium Titanate Nanotubes on a Titanium Metal Template. *Langmuir*, Vol. 23, pp. 2815-2823.

Yada, M.; Inoue, Y.; Uota, M.; Torikai, T.; Watari, T.; Noda, I. & Hotokebuchi, T. (2008). Formation of Sodium Titanate Nanotube Films by Hydrothermal Transcription. *Chemistry of Materials*, Vol. 20, pp. 364-366.

Yada, M.; Inoue, Y.; Gyoutoku, A.; Noda, I.; Torikai, T.; Watari, T. & Hotokebuchi, T. (2010). Apatite-forming ability of titanium compound nanotube thin films formed on a titanium metal plate in a simulated body fluid. *Colloids and Surfaces B: Biointerfaces*, Vol. 80, pp. 116-124.

Yamanaka, S.; Hamaguchi, T.; Muta, H.; Kurosaki, K. & Uno, M. (2004). Fabrication of Oxide Nanohole Arrays by a Liquid Phase Deposition Method. *Journal of Alloys and Compounds*, Vol. 373, pp. 312-315.

Yang, J.; Jin, Z.; Wang, X.; Li, W.; Zhang, S.; Guo, X. & Zhang, Z. (2003). Study on composition, structure and formation process of nanotube $Na_2Ti_2O_4(OH)_2$. *Journal of the Chemical Society Dalton Transactions*, Vol. 3, pp. 3898-3901.

Zhu, H. Y.; Lan, Y.; Gao, X. P.; Ringer, S., P.; Zheng, Z. F.; Song, D. Y. & Zhao, J. C. (2005). Phase Transition between Nanostructures of Titanate and Titanium Dioxides via Simple Wet-Chemical Reactions. *Journal of the American Ceramic Society*, Vol. 127, pp. 6730-6736.

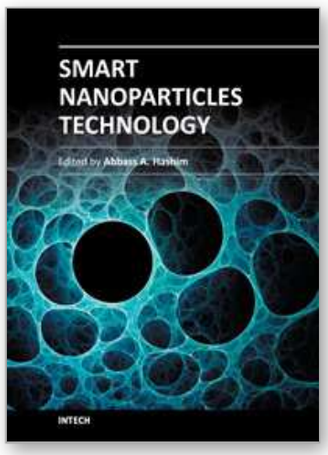

Smart Nanoparticles Technology

Edited by Dr. Abbass Hashim

ISBN 978-953-51-0500-8
Hard cover, 576 pages
Publisher InTech
Published online 18, April, 2012
Published in print edition April, 2012

In the last few years, Nanoparticles and their applications dramatically diverted science in the direction of brand new philosophy. The properties of many conventional materials changed when formed from nanoparticles. Nanoparticles have a greater surface area per weight than larger particles which causes them to be more reactive and effective than other molecules. In this book, we (InTech publisher, editor and authors) have invested a lot of effort to include 25 most advanced technology chapters. The book is organised into three well-heeled parts. We would like to invite all Nanotechnology scientists to read and share the knowledge and contents of this book.

How to reference

In order to correctly reference this scholarly work, feel free to copy and paste the following:

Mitsunori Yada and Yuko Inoue (2012). Synthesis of Titanate and Titanium Dioxide Nanotube Thin Films and Their Applications to Biomaterials, Smart Nanoparticles Technology, Dr. Abbass Hashim (Ed.), ISBN: 978-953-51-0500-8, InTech, Available from: http://www.intechopen.com/books/smart-nanoparticles-technology/synthesis-of-titanate-and-titanium-dioxide-nanotube-thin-films-and-their-applications-to-biomaterial

INTECH
open science | open minds

InTech Europe
University Campus STeP Ri
Slavka Krautzeka 83/A
51000 Rijeka, Croatia
Phone: +385 (51) 770 447
Fax: +385 (51) 686 166
www.intechopen.com

InTech China
Unit 405, Office Block, Hotel Equatorial Shanghai
No.65, Yan An Road (West), Shanghai, 200040, China
中国上海市延安西路65号上海国际贵都大饭店办公楼405单元
Phone: +86-21-62489820
Fax: +86-21-62489821

IntechOpen